materials

MDPI

Article

Bimetallic Co-Based (CoM, M = Mo, Fe, Mn) Coatings for High-Efficiency Water Splitting

Jadranka Milikić [1], Aldona Balčiūnaitė [2], Zita Sukackienė [2], Dušan Mladenović [1], Diogo M. F. Santos [3], Loreta Tamašauskaitė-Tamašiūnaitė [2] and Biljana Šljukić [1,3,*]

1 Faculty of Physical Chemistry, University of Belgrade, Studentski trg 12–16, 11158 Belgrade, Serbia; jadranka@ffh.bg.ac.rs (J.M.); dusan.mladenovic@ffh.bg.ac.rs (D.M.)
2 Department of Catalysis, Center for Physical Sciences and Technology, Saulėtekio ave. 3, Vilnius LT-10257, Lithuania; aldona.balciunaite@ftmc.lt (A.B.); zita.sukackiene@ftmc.lt (Z.S.); loreta.tamasauskaite@ftmc.lt (L.T.-T.)
3 Center of Physics and Engineering of Advanced Materials, Instituto Superior Técnico, Universidade de Lisboa, 1049-001 Lisbon, Portugal; diogosantos@tecnico.ulisboa.pt
* Correspondence: biljka@ffh.bg.ac.rs or biljana.paunkovic@tecnico.ulisboa.pt

Abstract: Bimetallic cobalt (Co)-based coatings were prepared by a facile, fast, and low-cost electroless deposition on a copper substrate (CoFe, CoMn, CoMo) and characterized by scanning electron microscopy with energy dispersive X-ray spectroscopy and X-ray diffraction analysis. Prepared coatings were thoroughly examined for hydrogen evolution reaction (HER) and oxygen evolution reaction (OER) in alkaline solution (1 M potassium hydroxide, KOH) and their activity compared to that of Co and Ni coatings. All five coatings showed activity for both reactions, where CoMo and Co showed the highest activity for HER and OER, respectively. Namely, the highest HER current density was recorded at CoMo coating with low overpotential (61 mV) to reach a current density of 10 mA·cm^{-2}. The highest OER current density was recorded at Co coating with a low Tafel slope of 60 mV·dec^{-1}. Furthermore, these coatings proved to be stable under HER and OER polarization conditions.

Keywords: electroless deposition; cobalt-based coatings; hydrogen evolution reaction; oxygen evolution reaction; water electrolysis

check for updates

Citation: Milikić, J.; Balčiūnaitė, A.; Sukackienė, Z.; Mladenović, D.; Santos, D.M.F.; Tamašauskaitė-Tamašiūnaitė, L.; Šljukić, B. Bimetallic Co-Based (CoM, M = Mo, Fe, Mn) Coatings for High-Efficiency Water Splitting. *Materials* **2021**, *14*, 92. https://doi.org/10.3390/ma14010092

Received: 2 December 2020
Accepted: 23 December 2020
Published: 28 December 2020

Publisher's Note: MDPI stays neutral with regard to jurisdictional claims in published maps and institutional affiliations.

Copyright: © 2020 by the authors. Licensee MDPI, Basel, Switzerland. This article is an open access article distributed under the terms and conditions of the Creative Commons Attribution (CC BY) license (https://creativecommons.org/licenses/by/4.0/).

1. Introduction

The electrochemical water splitting is a simple method to produce high purity hydrogen (H_2) through cathodic reaction (hydrogen evolution reaction, HER) and on the other side, oxygen (O_2) through anodic reaction (oxygen evolution reaction, OER) [1–5]. H_2 gas produced by water electrolysis could be a great replacement for fossil fuels such as coal and petroleum as its consumption produces no carbon dioxide (CO_2) or other greenhouse gasses [6]. Hence, the number of studies related to water electrolysis has increased significantly every year during the last decade, aiming to increase the process efficiency and decrease its cost [7–12]. OER proceeding via a 4-electron pathway is slower than HER proceeding via a 2-electron pathway [6]. Platinum (Pt) showed the best catalytic activity for HER, while iridium oxide (IrO_2) and ruthenium oxide (RuO_2) were presented as the best electrocatalysts for OER in alkaline media with low overpotential [1,13]. The major limitations of these electrocatalysts are their high cost, low abundance, and low catalytic stability. It is very important to find appropriate low-cost electrocatalysts that can improve HER and OER kinetics and efficiency. Transition metal-based electrocatalysts combined with noble metals are presented as good electrocatalysts for both HER and OER in alkaline media [14,15]. Also, transition metal phosphides [16,17], sulfides [18,19], selenides [20,21], carbides [22,23] and nitrides [24] have been tested as bifunctional electrocatalysts for HER and OER.

Strained cobalt(II) oxide (S-CoO) exhibited a Tafel slope of 94 mV·dec^{-1}, confirming the Heyrovsky–Volmer HER mechanism [25]. Incorporation of a small amount of copper (Cu) impurities into Co_3O_4 precursor led to the formation of Co_3O_4–CuO nanowires and resulted in improved conductivity as well as good catalytic activity for HER [26]. This mixed transition metal oxide gave a current density of 10 mA·cm^{-2} at 0.288 V vs. reversible hydrogen electrode (RHE) and Tafel slope of 65 mV·dec^{-1} [26]. Fe- and Mn-doped CoP electrocatalysts were tested for HER in 1 M potassium hydroxide (KOH) with a low overpotential of 163 mV·dec^{-1} observed for HER at CoP–FeP [2]. The excellent activity of CoP–FeP for HER could be a consequence of the optimized electronic structure of Co centers and P upon the introduction of Fe [2]. $Co_{0.85}Se$/nitrogen-doped graphene showed small Tafel slopes of 76.5 mV·dec^{-1} with a low HER onset potential of 111 mV in 1 M KOH [21]. A hybrid electrocatalyst of FeCo alloy nanoparticles deposited on a porous N-doped carbon (FeCo-TA@CMS) was also tested for HER in alkaline media where Tafel slope value of 102 mV·dec^{-1} revealed that the Volmer process is the rate-controlling step [27]. Factors affecting HER activity of bimetallic nickel M_xNi_{1-x} (M = Cr, Mo, and W; x = 0.2) alloys were defined by density functional theory (DFT) revealing that OH species on the surface preferred to adsorb on the top site of the M element, which could change the hydrogen adsorption energy (ΔG_H^*) on the active site [28].

As for OER, Co-based materials could easily form hydroperoxo (-OOH) species and after that deprotonate to O_2 formation [29]. Co-, Co_xFe-, and Fe-metal-organic frameworks (MOFs) with different Co/Fe molar ratios were tested for OER in 1 M KOH [30]. Co_2Fe–MOF presented the best electrocatalytic activity for OER with low overpotential at 10 mA·cm^{-2} (280 mV) and low Tafel slope (44.7 mV·dec^{-1}) [30]. Ag_2S–CoS heteronanowires showed excellent OER activity with an overpotential of 275 mV, low charge transfer resistance, and high electrical conductivity due to the octahedral Co sites as active sites for the OER in 1 M KOH [6]. Tafel slopes of 52, 66, and 60 mV·dec^{-1} were obtained for OER at the activated multishell Mn–Co oxyphosphide, Mn–Co oxyphosphide, and Mn–Co oxide particles, respectively, in 1 M KOH [16]. These metal phosphide-based materials showed that during the electrochemical process, the oxyphosphides are oxidized to oxide or hydroxide species presenting active sites for OER [16]. Post-phosphorization treatment of $NiMoO_4$ (P-NMO) induced new active sites and resulted in improved performance for OER in alkaline solution so that OER onset potential at 5 mA·cm^{-2} (370 mV) was lower than that of IrO_2 (390 mV) along with lower Tafel slope (70.3 mV·dec^{-1}) [31]. A three-dimensional self-operated Co-doped nickel selenide nanoflowers (3D Co–NiSe/NF) electrode showed low OER overpotential with Tafel slope of 111 mV·dec^{-1} in 1 M KOH [32].

Transition metal-based materials, such as molybdenum disulfide (MoS_2) synthesized by the hydrothermal method, showed to be bifunctional electrocatalysts for water splitting with high HER and OER activities [1]. Furthermore, iron selenide on Ni foam (FeSe–NF) proved to be a good electrocatalyst for HER and OER in 1 M KOH [33] with the lowest OER onset potential (ca. 150 mV) compared to Se–NF (190 mV), Fe–NF (300 mV) and NF (320 mV) [33]. Tafel slopes of 201, 181, 155 and 145 mV·dec^{-1} were obtained during HER at NF, Se–NF, Fe–NF and FeSe–NF, respectively. Ni–Co alloy nanostructured electrodes with four different amounts of Ni and Co were also examined for both HER and OER in KOH aqueous solution. Ni–Co nanowires with ca. 95% of Co and 5% of Ni showed the highest HER and OER activity with a low potential of –0.231 V and 1.494 V required to attain a current density of 10 mA·cm^{-2} for HER and OER, respectively [34].

In this work, Co-based bimetallic coatings (CoM, M = Fe, Mn, Mo), as well as monometallic Co and Ni coatings, were prepared by a facile, fast, and low-cost electroless deposition method. The morphology and composition of prepared coatings were explored by scanning electron microscopy (SEM) with energy dispersive X-ray spectroscopy (EDX), X-ray diffraction analysis and inductively coupled plasma–optical emission spectrometry (ICP–OES) analysis. The effect of combining Co with left-hand side transition metals on activity for HER and OER in alkaline media (1 M KOH) was then systematically studied

by linear sweep voltammetry (LSV), cyclic voltammetry (CV), electrochemical impedance spectroscopy (EIS), and chronoamperometry (CA).

2. Experimental

2.1. Preparation of Coatings

Electroless deposition of Co was performed on the copper (Cu) surface. Prior to electroless deposition of Co, Cu sheets (1 cm × 1 cm) were pre-treated with 50–100% calcium magnesium oxide, known as "Vienna Lime" (Kremer Pigmente GmbH & Co. KG, Aichstetten, Germany), and rinsed with deionized water. Cu sheets were then activated with Pd(II) ions by immersion in 0.5 $g \cdot L^{-1}$ $PdCl_2$ solution for 10 s and again rinsed with deionized water. Activated Cu sheets were placed into the electroless cobalt plating bath containing 0.05 M cobalt sulfate ($CoSO_4$), 0.05 M morpholine borane ($C_4H_8ONH \cdot BH_3$), and 0.2 M glycine (NH_2CH_2COOH). The bath operated at pH 7 at a temperature of 30 °C for 30 min. The thickness of the pure Co coating was determined gravimetrically and it was found to be ca. 1 µm. The deposition conditions for the rest of the coatings are presented in Table 1. Salts used were $Na_2MoO_4 \cdot 2H_2O$ (≥99.5%), $FeSO_4 \cdot 7H_2O$ (≥99%), $MnSO_4 \cdot H_2O$ (≥99%), and $NiSO_4 \cdot 6H_2O$ (≥98%), all from Sigma–Aldrich (Taufkirchen, Germany).

Table 1. Deposition conditions during the preparation of the herein studied coatings.

	Deposition Conditions										
Coating	**$CoSO_4$/M**	**Morpholine Borane/M**	**Glycine/M**	**Mo^{6+}/mM**	**Fe^{2+}/mM**	**Mn^{2+}/mM**	**Ni^{2+}/mM**	**Trisodium Citrate/mM**	**pH**	**T/°C**	**t/min**
Co	0.05	0.05	0.2	-	-	-	-	-	7	30	30
CoMo	0.1	0.2	-	1	-	-	-	-	7	60	30
CoFe	0.07	0.06	0.2	-	5	-	-	18	7	50	30
CoMn	0.07	0.06	0.2	-	-	5	-	18	7	50	30
Ni	-	0.02	0.2	-	-	-	50	40	7	30	30

2.2. Characterization of CoM (M = Fe, Mn, Mo), Co and Ni Coatings

The morphology and composition of the prepared coatings were investigated by scanning electron microscopy (SEM) using a SEM/FIB workstation Helios Nanolab 650 (Hillsboro, OR, USA) with an energy dispersive X-ray (EDX) spectrometer INCA Energy 350 X-Max 20 (Oxford Instruments, Abingdon, UK).

The coatings' composition and structure were further confirmed by X-ray diffraction (XRD) analysis with diffraction data collected using Rigaku Ultima IV diffractometer in Bragg–Brentano geometry over the scattering angle 2θ range 20–80°.

Mass of the elements and metal loadings were determined by inductively coupled plasma optical emission spectrometry (ICP–OES) analysis. Prior to the analysis, all the prepared coatings were dissolved in HCl solution and diluted up to 10 mL. The ICP–OES spectra were recorded using an Optima 7000DV spectrometer (Perkin Elmer, Waltham, MA, USA) at wavelengths of λ_{Co} 228.616 nm, λ_{Co} 238.892 nm, λ_B 249.677 nm, λ_{Mo} 202.031 nm, λ_{Mo} 203.845 nm, λ_{Fe} 238.204 nm, λ_{Mn} 257.610 nm, and λ_{Ni} 231.604 nm.

2.3. Electrochemical Measurements

All electrochemical measurements were done using Ivium V01107 potentiostat (Eindhoven, The Netherlands) in a three-electrode system with saturated calomel (SCE) as a reference, graphite rod as counter and CoM (M = Fe, Mn, Mo), Co or Ni as the working electrode, in 1 M potassium hydroxide (KOH) as supporting electrolyte. All potentials in this work were converted to the reversible hydrogen electrode (RHE) scale using the following equation: $E_{RHE} = E_{SCE} + 0.242\ V + 0.059\ V \times pH_{solution}$. Current densities were calculated using the electrodes' geometric area of 1 cm^2.

CVs were recorded from 1.02 to 1.22 V, at different polarization rates in the range from 5 to 100 $mV \cdot s^{-1}$ in 1 M KOH saturated with nitrogen (N_2).

HER polarization curves were recorded from the open circuit potential (OCP) to −0.38 V at a polarization rate of 5 $mV \cdot s^{-1}$. HER electrochemical impedance spectroscopy (EIS) analysis was conducted in the frequency range of 100 kHz to 0.1 Hz, with 5 mV amplitude at a potential of −0.33 V.

OER polarization curves were recorded from OCP to 2.12 V at a polarization rate of 5 $mV \cdot s^{-1}$. OER EIS measurements were done at a potential of 1.67 V with an amplitude of 5 mV in the 100 kHz–0.1 Hz range.

Polarization curves and EIS measurements were recorded at several temperatures from 25 to 85 °C, setting the temperature with a water jacket connected to a Haake water bath.

Stability was studied by recording chronoamperometry (CA) curves under HER (potential of −0.24 V) and under OER (potential of 1.67 V) conditions for 1 h for all coatings and then for 24 h for the coatings that showed the highest HER/OER activity.

3. Results

3.1. Characterization of Coatings

Mass of the elements deposited onto Cu substrate surface and their loadings, determined by ICP–OES analysis, are given in Table 2. It can be seen that the formed Co, CoMo, CoFe, and CoMn coatings contained more than 90 wt.% of Co and between 0.64–1.8 wt.% of B. In the case of Ni coating, it contained more than 97 wt.% of Ni and ~3 wt.% of boron (B).

Table 2. Mass of the elements and total metal loading in the coatings as determined by inductively coupled plasma optical emission spectrometry (ICP–OES) analysis.

Coating	Mass of Element/mg						Total Metal Loading/$mg \cdot cm^{-2}$
	Co	B	Mo	Fe	Mn	Ni	
Co	2.027	0.01413	-	-	-	-	1.02057
CoMo	3.198	0.06367	0.2275	-	-	-	1.74459
CoFe	0.5472	0.00384	-	0.05282	-	-	0.30193
CoMn	3.064	0.02331	-	-	0.0017	-	1.54451
Ni	-	0.01591	-	-	-	0.525	0.27046

SEM analysis revealed somewhat different morphology of the prepared coatings (Figure 1A–E), with EDX analysis verifying uniform distribution of components. Namely, layers of the prepared catalysts were polycrystalline, but with particles of different sizes exhibiting agglomerates of oval structure. Surface morphology plays an important role in electrocatalysis as it determines both the contact surface area as well as the number of edge active sites where the charge distribution is localized [35]. Furthermore, it plays an important role in the generation of H_2/O_2 gas bubbles that might block access to the active sites [36]. In the competition between the nucleation and growth of gas bubbles, a flat surface will favor the growth process leading to the formation of large bubbles, while cracks will limit the growth of O_2 bubbles within them [36,37].

The compositions of the five coatings were further investigated by XRD analysis (Figure 1F). In case of the Ni and CoFe coatings, with low metal loading, the peaks related to the Cu substrate are also visible at 2θ of ca. 43.5, 50.5 and 74.2°, overlapping with the reflections from the Ni (111), (200) and (220) planes, respectively, and Co (002), (101) and (110) planes, respectively [5].

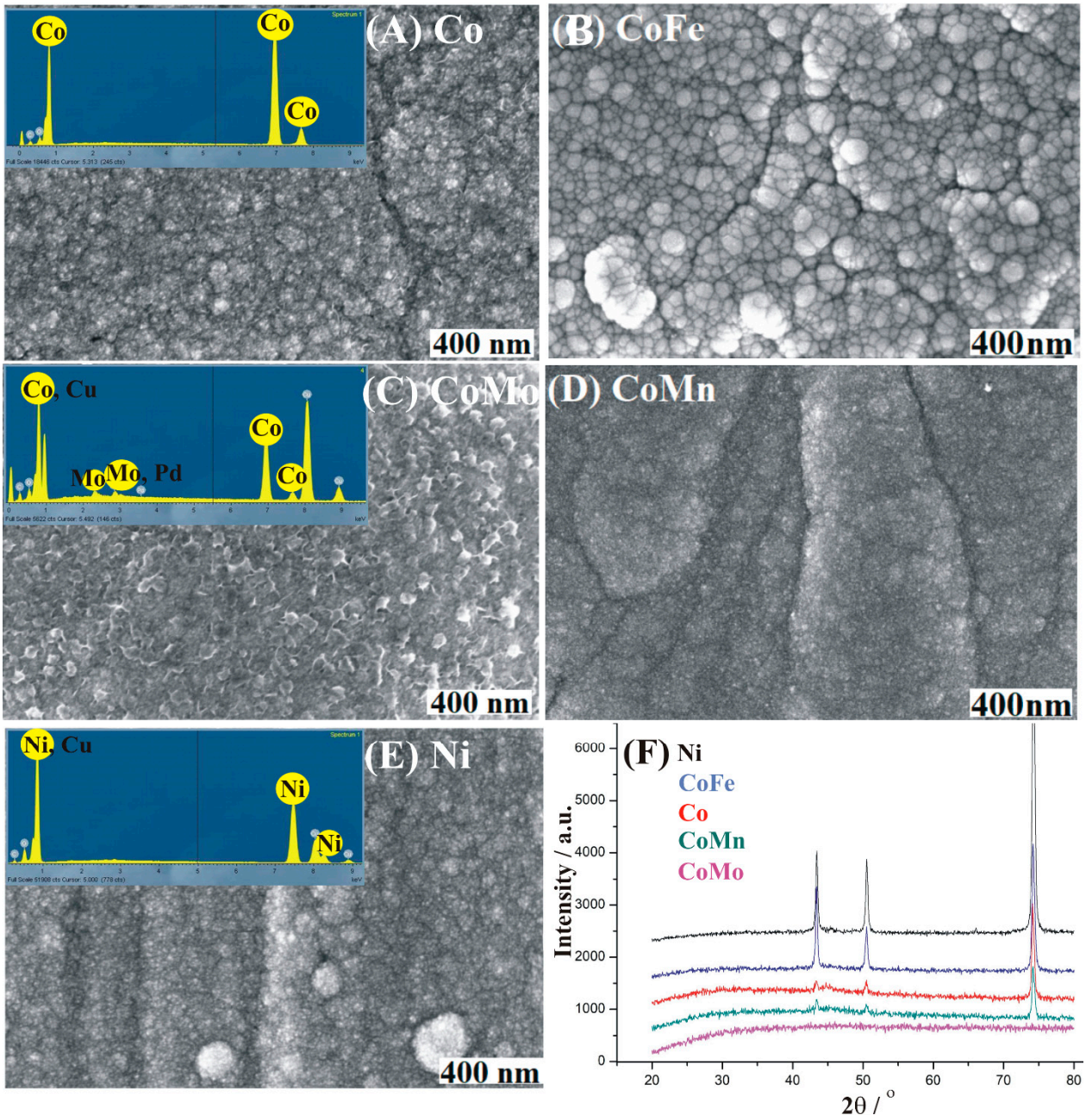

Figure 1. (**A**–**E**) SEM images (with EDX spectra in inset of (**A**,**C**,**E**)) of the five prepared coatings and (**F**) their XRD patterns.

Electrochemical characterization of coatings was conducted by recording CVs in N_2-saturated 1 M KOH at different polarization rates (not shown). These results were used for the investigation of charge storage capability of the studied coatings, i.e., for determination of their double-layer capacitance (C_{dl}), which is proportional to their electrochemical active surface area (ECSA) [38–40]. Namely, adsorption of H and O (underpotential deposition) on the electrode material's surface is a requirement for HER and OER, respectively [41]. CVs at different polarization rates indicate the rate capability of an electrode material, i.e., its efficiency to adsorb a substantial H/O amount and desorb with a high coulombic efficiency. C_{dl} was found to decrease in order CoMo (21.2 $\mu F \cdot cm^{-2}$) > Ni (21.0 $\mu F \cdot cm^{-2}$) > CoFe (6.2 $\mu F \cdot cm^{-2}$) > CoMn (3.0 $\mu F \cdot cm^{-2}$) > Co (2.1 $\mu F \cdot cm^{-2}$), with a value of 20 $\mu F \cdot cm^{-2}$ being reported as average C_{dl} value of a smooth metal surface [42]. C_{dl} values several times higher for CoMo and Ni than C_{dl} values of CoFe, CoMn, and Co coatings reflected the notably higher number of active sites at the former that could take part in the adsorption

processes and lead to higher HER electrocatalytic activity. Nevertheless, the electrocatalytic reactivity of the active sites depends on their accessibility as well as their oxidation state.

3.2. Hydrogen Evolution Reaction Study

HER activity of studied coatings was evaluated in 1 M KOH by LSV method. CoMo gave the highest current density (j), followed by CoMn and Co coatings, and then by CoFe and Ni with notably lower current density during HER (Figure 2A). For instance, the current densities of −124.2, −74.1, −67.1, −16.6 and −9.5 mA·cm^{-2} were reached at −0.3 V using CoMo, CoMn, Co, CoFe, and Ni coatings, respectively. Overpotential to reach current density of 10 mA cm^{-2} (η_{10}) was found to be as low as 61 mV for CoMo and increased in the order CoMo (61 mV) < CoMn (238 mV) < Co (246 mV) < CoFe (285 mV) < Ni (308 mV).

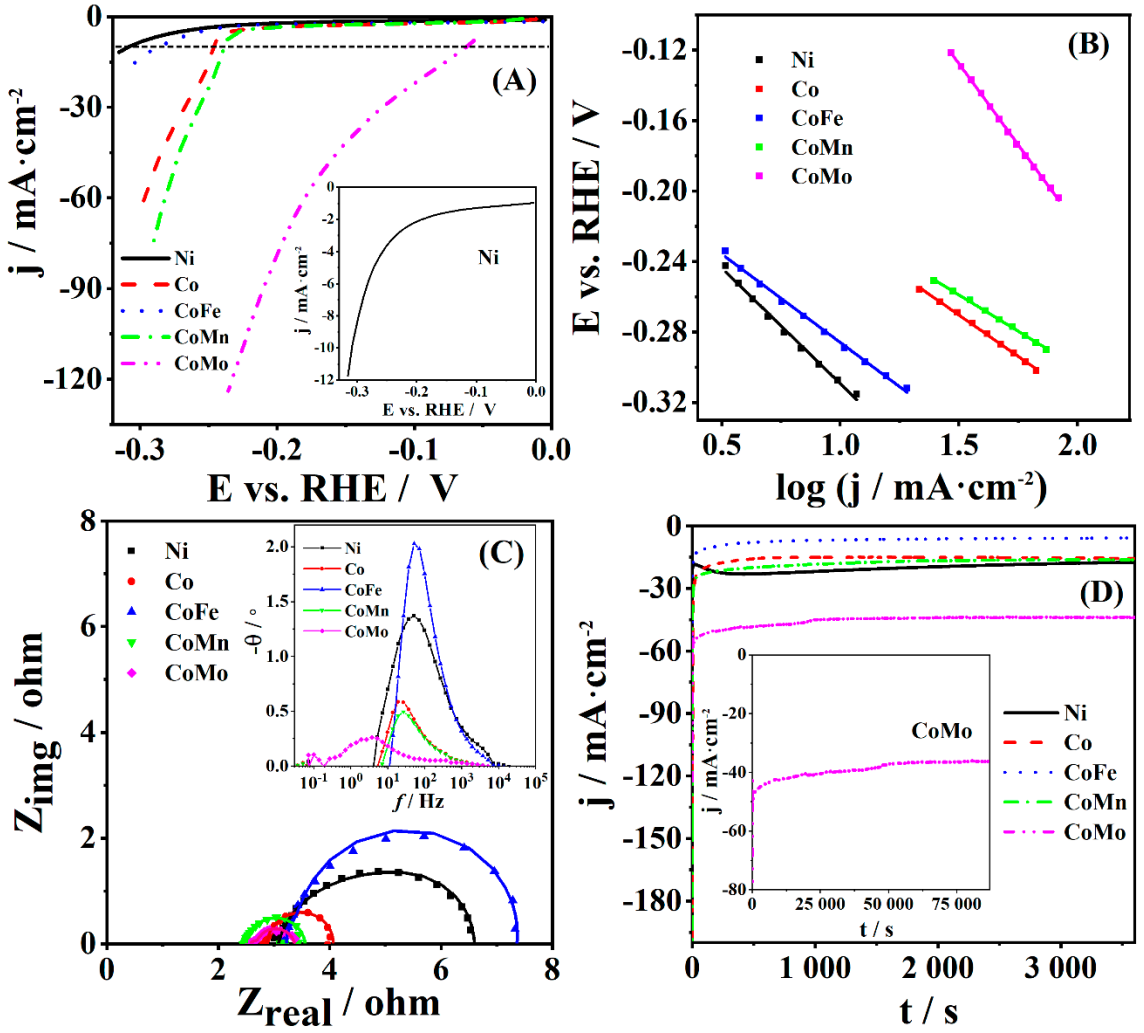

Figure 2. (**A**) Hydrogen evolution reaction (HER) polarization curves (iR-corrected) of five studied coatings at 5 mV·s^{-1} with (**B**) corresponding Tafel plots, (**C**) Nyquist plots at −0.33 V (amplitude of 5 mV in the 100 kHz–0.1 Hz range) with the corresponding Bode plots in the inset, and (**D**) chronoamperometric curves at −0.24 V for 1 h with the chronoamperometric curve of CoMo at the same potential for 24 h (inset). All measurements were done in 1 M KOH.

The HER kinetics was explored by Tafel analysis (Figure 2B), i.e., determination of Tafel slope (b) as a measure of a rate at which current density increases with the increase of overpotential, and exchange current density (j_0), reflecting the electrode's intrinsic activity for HER. Tafel slope values were found to be 83, 94, 100, 131, and 184 mV·dec^{-1} (Table 3) for CoMn, Co, CoFe, Ni, and CoMo, respectively. The exchange current density (j_0) was

calculated for HER at all five coatings by extrapolation of the Tafel plots, η vs. log j. Thus, j_0 of 0.31, 0.04, 0.04, 0.02 and 0.01 mA·cm^{-2} were calculated for CoMo, Ni, Co, CoMn, and CoFe, respectively (Table 3). It is worth noting that the j_0 value determined for HER at CoMo coating was ca. seven times higher than that determined for the rest of the studied coatings.

Table 3. Electrochemical performance of the tested coatings toward HER in alkaline media.

Coating	Tafel Slope (mV·dec^{-1})	j_0 (mA·cm^{-2})	η_{10} (mV)	R_{ct} (Ω)	Electrolyte
CoFe	100	0.02	285	2.10	1 M KOH
CoMn	83	0.02	238	1.03	1 M KOH
CoMo	184	0.31	61	1.15	1 M KOH
Co	94	0.04	246	2.80	1 M KOH
Ni	131	0.04	308	1.07	1 M KOH

The EIS measurements were used for additional investigation of the coating/electrolyte interface and the related processes occurring at the coating surface under HER conditions in 1 M KOH. Figure 2C shows the Nyquist and Bode (inset) plots of the five coatings. The solution resistance (R_s) (2.48–3.20 Ω range), as well as the charge transfer resistance (R_{ct}) (1.08–2.80 Ω range), were calculated using the equivalent circuit presented in Scheme 1 and found to be comparable for the studied coatings (Table 4).

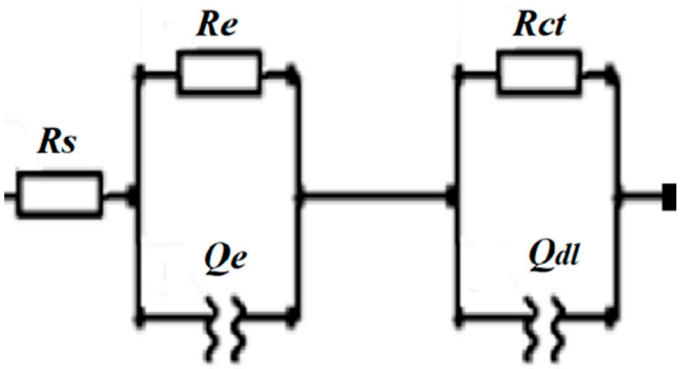

Scheme 1. Equivalent electric circuit used to fit the electrochemical impedance spectroscopy (EIS) data, where R_s is the electrolyte resistance, R_e is the electronic resistance of the material and the associated capacitance R_{ct} is the resistance of the charge transfer reaction, Q_e is the constant phase element, and Q_{dl} is an ideal double-layer capacitor.

Table 4. EIS parameters of the herein prepared coatings in 1 M KOH at –0.33 V (amplitude of 5 mV in the 100 kHz–0.1 Hz range).

Coating	R_s (Ω)	R_e (Ω)	R_{ct} (Ω)	Q_e (mF)	Q_{dl} (mF)
CoMo	2.56	6.60	1.15	100.0	40.0
CoFe	3.20	3.90	2.10	0.4	0.4
CoMn	2.48	0.02	1.03	637.4	6.8
Co	2.85	0.43	2.80	16.9	6.9
Ni	3.06	2.42	1.07	1.8	3.3

R_s—the electrolyte resistance, R_e—the electronic resistance of the material and the associated capacitance, R_{ct}—resistance of the charge transfer reaction, Q_e—the constant phase element, Q_d—the ideal double-layer capacitor.

Another crucial criterion for an advanced electrode material is its electrochemical stability. Chronoamperometric measurements with five coatings were done in 1 M KOH at −0.24 V for 1 h. CA results confirmed the result of LSV analysis in terms of CoMo giving the highest current density (−50.2 mA·cm^{-2} at 200 s) during HER (Figure 2D). More than two times lower current density was recorded with Ni (−22.4 mA·cm^{-2}), CoMn

(-21.7 mA·cm^{-2}) and Co (18.2 mA·cm^{-2}) coatings and notably lower value with CoFe (-5.7 mA·cm^{-2}). Activity for HER of all coatings (in terms of the recorded current density) was found to be stable during one-hour measurement. Thus, current density under HER conditions at CoMo decreased ca. 13% after 1 h. Furthermore, CoMo showed relatively stable current density during 24 h with a decrease of ca. 18.6%. Thus, HER current density of CoMo was found to be -54.3 mA·cm^{-2} at 800 s and -44.2 mA·cm^{-2} at 86,400 s.

HER at five coatings was studied at temperatures ranging from 25 up to 85 °C. The current densities of CoMo increased from -124.2 to -164.8 mA·cm^{-2} with increasing temperature from 25 to 65 °C, respectively, and then somewhat decreased at 75 and 85 °C (e.g., to 156.3 mA·cm^{-2} at 85 °C). Ni and CoFe showed the same trend of increasing current densities with the increase of temperature, whereas CoMn and Co did not show a significant difference in current densities with increasing temperature during HER. Furthermore, Tafel slopes were calculated for HER at five studied coatings at different temperatures (Figure 3). A decrease of Tafel slope value with increasing temperature was observed, e.g., Tafel slope for HER at CoMo was determined to be 184 and 126 mV·dec^{-1} at 25 and 85 °C, respectively.

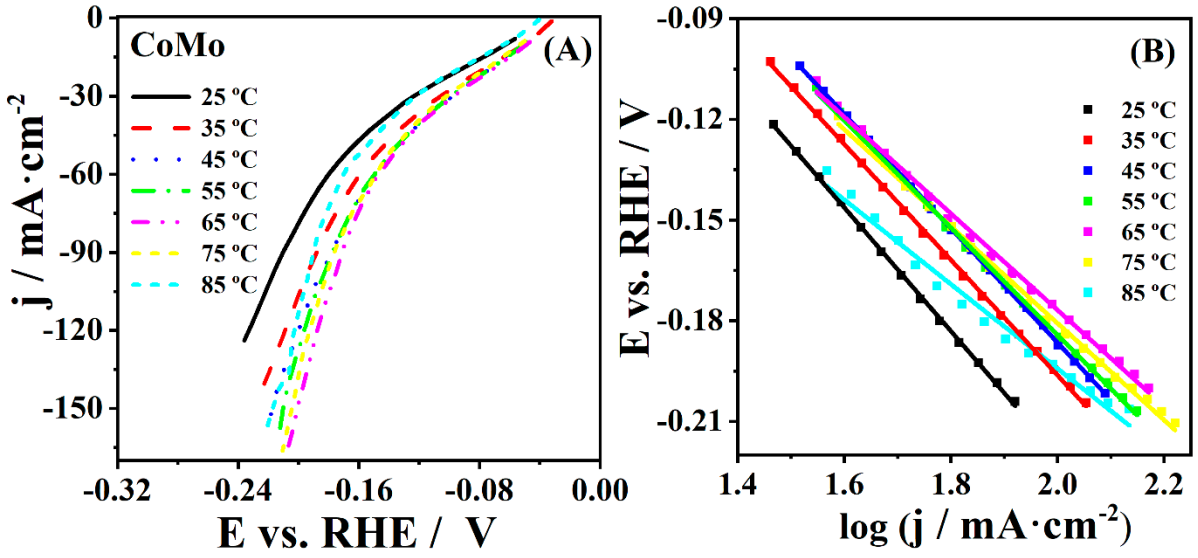

Figure 3. (**A**) HER polarization curves of CoMo coatings in 1 M KOH recorded at polarization rate of 5 mV·s^{-1} at different temperatures with (**B**) corresponding Tafel plots.

3.3. Oxygen Evolution Reaction

The activity of CoM (M = Fe, Mn, Mo), Co, and Ni coatings for oxygen evolution reaction was also thoroughly examined in alkaline media (1 M KOH). The polarization curves of studied coatings are presented in Figure 4, where it can be observed that the highest current density during OER was recorded at Co and CoMn, followed by CoFe and Ni, and then CoMo coating. An overpotential to reach a current density of 10 mA·cm^{-2} was found to be similar for Co (438 mV), CoMn (431 mV) and CoMo (431 mV) and ca. 120 mV higher for CoFe (553 mV) and Ni (559 mV) coatings (Table 5). Furthermore, the current density of 150 mA·cm^{-2} was reached at potential increasing in the following order Co (1.77 V) > CoMn (1.79 V) > Ni (1.86 V) > CoFe (1.92 V). Current density at CoMo coating did not reach a value of 150 mA cm^{-2} in the investigated potential range; it reached a value of only 99 mA cm^{-2} at 1.90 V.

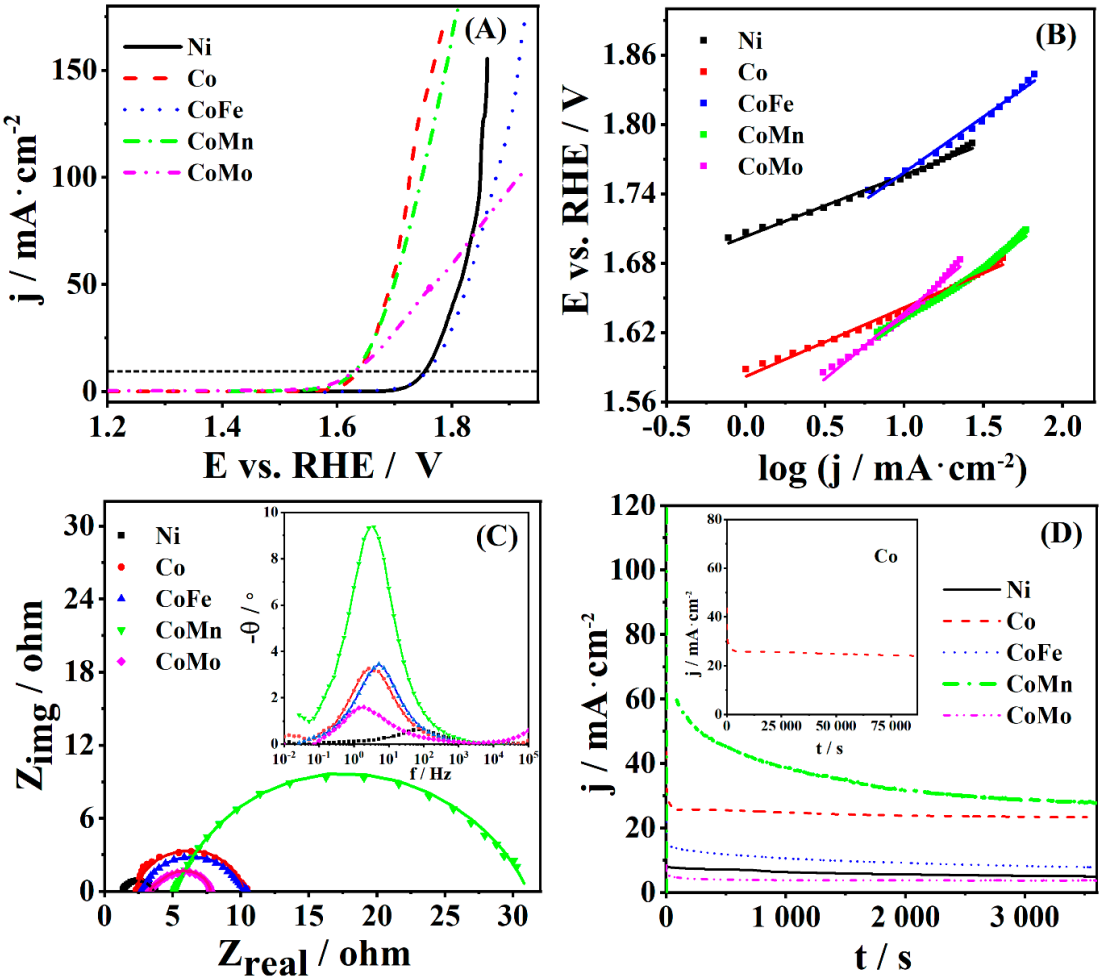

Figure 4. (**A**) Oxygen evolution reaction (OER) polarization curves (iR-corrected) of five studied coatings at 5 mV·s^{-1} with (**B**) corresponding Tafel plots, (**C**) Nyquist plots at 1.67 V (amplitude of 5 mV in the 100 kHz–0.1 Hz range) with the corresponding Bode plots in the inset, and (**D**) chronoamperometric curves at 1.67 V for 1 h with the chronoamperometric curve of Co coating at the same potential for 24 h (inset). All measurements were done in 1 M KOH.

Table 5. Electrochemical performance of the tested coatings toward OER in alkaline media.

Coating	Tafel Slope (mV dec^{-1})	η_{10} (mV)	R_{ct} (Ω)	Electrolyte
CoFe	96	559	7.44	1 M KOH
CoMn	94	431	20.16	1 M KOH
CoMo	114	431	1.01	1 M KOH
Co	60	438	7.9	1 M KOH
Ni	53	553	2.24	1 M KOH

OER polarization curves were then further used for constructing the Tafel plots and calculating the Tafel slope. Tafel slope values of 53 and 60 mV·dec^{-1} were found for OER at Ni and Co, respectively. Higher values of 94, 96, and 114 mV·dec^{-1} were determined for OER at CoMn, CoFe, and CoMo, respectively.

To get a deeper insight into the OER kinetics at studied coatings, EIS analysis was also performed in 1 M KOH under the OER conditions. Figure 4C shows the Nyquist plots at 1.67 V (amplitude of 5 mV in the 100 kHz–0.1 Hz range) and the Bode plots (inset of the figure) of the five coatings with R_{ct} determined (using the equivalent circuit presented in Scheme 1) to be 1.01, 2.24, 7.44, 7.90, and 20.16 Ω for CoMo, Ni, CoFe, Co, and CoMn coatings, respectively (Table 6). Furthermore, Co coating showed a favorable C_{dl} value of 9.6 mF.

Table 6. EIS parameters of OER at the studied coatings in 1 M KOH at 1.67 V (amplitude of 5 mV in the 100 kHz–0.1 Hz range).

Coating	R_s (Ω)	R_e (Ω)	R_{ct} (Ω)	Q_e (mF)	Q_{dl} (mF)
CoMn	5.16	25.5	20.2	3.0	1.0×10^{-10}
CoFe	2.38	3.10	7.44	1.0×10^{-10}	7.1
CoMo	3.29	3.44	1.01	32	25
Co	0.45	1.82	7.90	8.3×10^{-3}	9.6
Ni	0.02	1.29	2.24	1.7×10^{-4}	4.3

R_s—the electrolyte resistance, R_e—the electronic resistance of the material and the associated capacitance, R_{ct}—resistances of the charge transfer reaction, Q_e—the constant phase element, Q_{dl}—the ideal double-layer capacitor, W—Warburg element.

As mentioned, the electrode's electrochemical stability is another key criterion for the evaluation of its potential application. Figure 4D presents chronoamperometric curves of studied coatings at the potential of 1.67 V where the highest current density at 3600 s was recorded at CoMn (27.9 mA·cm^{-2}) and Co (23.5 mA·cm^{-2}), followed by CoFe (7.76 mA·cm^{-2}), Ni (5.08 mA·cm^{-2}) and CoMo (3.48 mA·cm^{-2}) coatings. Chronoamperometric curves of CoMn and CoFe coatings revealed somewhat lower stability of these two coatings as they showed a current density decrease of about 50 and 40%, respectively, when comparing the values in 180 and 3600 s. Co showed good stability during 24 h where current density decreased from 28.6 mA·cm^{-2} at 800 s to 25.5 mA·cm^{-2} at 27,700 s.

Additionally, the impact of temperature on OER activity of five studied coatings in 1 M KOH was thoroughly tested at temperatures ranging from 25 to 85 °C. A pronounced increase of current density with temperature was observed. Thus, the potential to reach a current density of 120 mA·cm^{-2} at Co coating decreased from 1.74 V at 25 °C to 1.52 V at 85 °C (Figure 5A). Figure 5B shows the corresponding Tafel plots of Co coating at different temperatures where Tafel slope values changed slightly; the same behavior was observed for the other coatings as well.

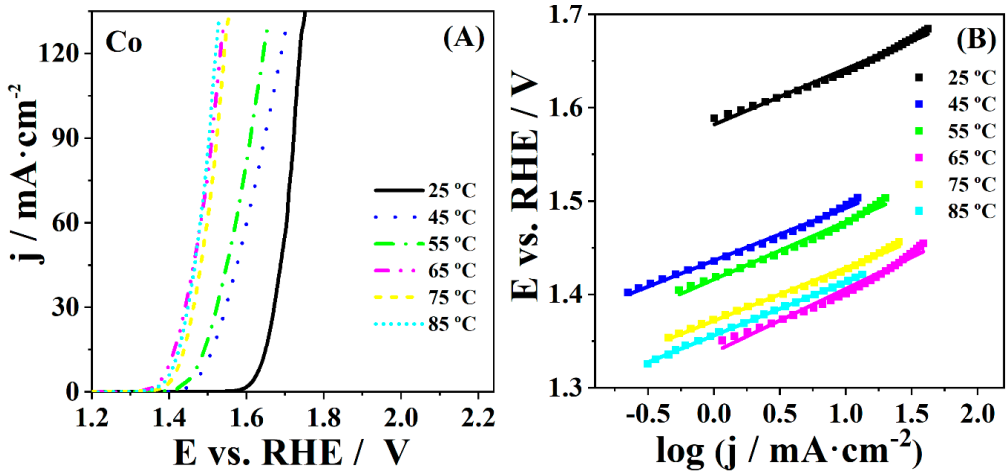

Figure 5. (**A**) OER polarization curves of Co coating in 1 M KOH recorded at polarization rate of 5 mV·s^{-1} at different temperatures with (**B**) corresponding Tafel plots.

4. Discussion

HER in alkaline solution proceeds by the following three steps:

$$M + H_2O + e^- \leftrightarrow MH_{ads} + OH^- \text{ (Volmer step, b = 120 mV·dec}^{-1}\text{)}, \quad (1)$$

$$MH_{ads} + H_2O + e^- \leftrightarrow H_2 + M + OH^- \text{ (Heyrovsky step, b = 40 mV·dec}^{-1}\text{)}, \quad (2)$$

$$MH_{ads} + MH_{ads} \leftrightarrow H_2 + 2M \text{ (Tafel step, b = 30 mV·dec}^{-1}\text{)}. \quad (3)$$

The Volmer step represents electrosorption of the hydrogen proton (H^+) to form the surface adsorbed hydrogen atom (MH_{ads}) on the active metal sites (M), the Heyrovsky step is the electrochemical desorption of MH_{ads} to form H_2, and the Tafel step represents recombination of two MH_{ads} on the metal surface to form H_2 [32,33]. Tafel slope values suggest that HER at CoMn, Co, and CoFe proceeds by the Volmer–Heyrovsky mechanism where the electrochemical desorption of the MH_{ads} is the rate-limiting step [32,34], while during HER at Ni and CoMo, the Volmer step, i.e., electrochemical sorption of H^+, represents the rate-determining step. It could be seen that the determined Tafel slope values deviated from the theoretical ones toward higher values that might have been caused by the formation of surface oxides of lower conductivity compared to the metallic surface [34].

The notably higher double-layer capacitance of CoMo coating could account for its higher activity toward HER compared to the other coatings. Furthermore, the overpotential value to reach the current density of 10 $mA \cdot cm^{-2}$ determined for CoMo was lower than the values of 73 and 288 mV reported for S-CoO nanorods [19,20] and Co_3O_4–CuO electrocatalyst [19,20], respectively (Table 7). It was also lower than the overpotential of 163.0 mV to achieve a current density of 10 $mA \cdot cm^{-2}$ for HER at CoP–FeP in alkaline electrolyte solution [2]. Furthermore, it was lower than the overpotential of 119 and 297 mV at 10 $mA \cdot cm^{-2}$ at Mo_2C@C and Ni foam, respectively [37,38].

Obtained results showed that the combination of Co as right-hand side transition metal with Mo as left-hand side transition metal results in enhancement of the coating's intrinsic activity. Material electrocatalytic activity for HER is governed by the H adsorption free energy [41]. The well-known volcano plot indicates noble metals as the best electrocatalysts for HER, while the activity of transition metals can be improved by combining multiple metals with different, weak and strong, bonds with hydrogen [43]. Consequently, metal forming a strong bond with H initiates the H adsorption, with the possibility of H_{ads} moving via surface diffusion. Metal forming a weak bond with H then facilitates the H_2 generation and its release from the electrode surface. Furthermore, the presence of a second metal of different size changes the lattice structure, which can result in the generation of active sites. Finally, a combination of two transition metals can improve the electrochemical stability compared to the components [41].

Table 7. Electrochemical performance of herein tested coatings towards HER in alkaline media and comparison with that of transition metal-based electrodes reported in the literature.

Electrode	Tafel Slope ($mV \cdot dec^{-1}$)	j_0 ($mA \cdot cm^{-2}$)	η_{10} (mV)	R_{ct} (Ω)	Electrolyte	Ref.
CoFe	100	0.02	285	2.10	1 M KOH	This work
CoMn	83	0.02	238	1.03	1 M KOH	This work
CoMo	184	0.31	61	1.15	1 M KOH	This work
Co	94	0.04	246	2.80	1 M KOH	This work
Ni	131	0.04	308	1.07	1 M KOH	This work
Co_3O_4-CuO	65	-	288	173.20	1 M KOH	[26]
Co_3O_4	94	-	-	384.50	1 M KOH	[26]
CuO	243	-	-	656.90	1 M KOH	[26]
P-CoO NRs *	164	-	208	-	1 M KOH	[25]
CoP-FeP	51.2	-	163	141	1 M KOH	[2]
Mo_2C@C	51	-	119	-	1 M KOH	[44]
Ni-rGO/Ni foam **	108	0.5	187	32.30	1 M NaOH	[45]
$Fe_{1.89}Mo_{4.11}O_7/MoO_2$	79	-	197	-	1 M KOH	[46]
Co_9S_8-MoS_2@3DC ***	83.6	-	177	41.42	1 M KOH	[47]
MoS_2@3DC	102.8	-	252	316.3	1 M KOH	[47]
Co_9S_8@3DC	97.1	-	242	162.4	1 M KOH	[47]

* NRs—nanorods, ** rGO—the reduced graphene oxide, *** 3DC—the three-dimensional interconnected hierarchical pore carbon.

As for the state of the surface, it has been suggested that the presence of oxides on the metal surface is crucial for HER activity due to the oxides' affinity to form OH_{ads} and thus promote water splitting [35]. Formed OH species adsorb on the metal oxide, while

H atoms formed adsorb at the neighboring metal active sites. Thus, adequate tailoring metal/metal oxide interfaces can lead to a bifunctional HER mechanism.

An OER Tafel slope value lower than 60 mV·dec^{-1} suggests a four-electron transfer determining step while a value higher than 60 mV·dec^{-1} suggests a three-electron transfer determining step [36], with increased multiple electron transfer process (case of Ni and Co), indicating better electrocatalytic performance of a coating. Tafel slope for OER at NiFeMo oxide catalyst was reported to be 64 mV·dec^{-1} [38] and at $NiCo_2O_4$ 89 mV·dec^{-1} [40] in 0.1 M KOH, i.e., higher than the values for herein tested Co coating (Table 8).

Overpotential at a current density of 10 mA·cm^{-2} values are somewhat higher than those given in the literature reports for OER at different transition metal-based electrodes (Table 8). Thus, CoMn, CoMo, and Co can be seen as good materials for OER, and CoFe and Ni as satisfactory ones [42]. Transition metals' activity towards OER is governed, among other factors, by the number and accessibility of active sites, their oxidation state (+2, +3, or +4), 3D electrons number, and surface oxygen binding energy [48]. Namely, OER is reported ideally not to be a surface reaction, but to occur in a ca. 10 nm layer of the electrode material [37]. Furthermore, it has been reported that parallel with the OER occurs the phase conversion of Co-based materials (metal to oxides, oxides to hydroxides or oxyhydroxides), taking an active role during OER. Active sites in their high oxidation state, with the transition occurring at potentials lower than that of OER via a pseudocapacitive behavior, will favor activity for the OER [37]. Incorporation of a second transition metal typically should boost the OER activity by altering intermediate bonds and electronic structure, and, thus, increasing the electric conductivity [49]. The strength of the OH_{ads}–$M^{2+\delta}$ bond increases in the order Ni < Co < Fe < Mn [50].

Table 8. Electrochemical performance of herein tested coatings toward OER in alkaline media and comparison with that of transition metal-based electrodes reported in the literature.

Electrode	Tafel Slope (mV·dec^{-1})	η_{10} (mV)	R_{ct} (Ω)	Electrolyte	Ref.
CoFe	96	559	7.44	1 M KOH	This work
CoMn	94	431	20.16	1 M KOH	This work
CoMo	114	431	1.01	1 M KOH	This work
Co	60	438	7.9	1 M KOH	This work
Ni	53	553	2.24	1 M KOH	This work
Co_3Fe-MOF	55.6	314	-	1 M KOH	[51]
$NiCoFeO_x$ NSs/NF basal growth NHS	61	260	1.52	1 M KOH	[3]
Ultrathin NiCoFeOx NSs/NF	84	305	-	1 M KOH	[3]
P-NMO	70.3	370 at 5 mA·cm^{-2}	-	1 M KOH	[31]
NMO	80.6	440 at 5 mA·cm^{-2}	-	1 M KOH	[31]
Co–P/NF-10	51.1	306	20	1 M KOH	[5]
c-NiFeMo	64	440	85	0.1 M KOH	[52]
$GFC20_{800}$	180	-	110.3	1 M KOH	[53]
$GFC20_{700}$	154	-	90.3	1 M KOH	[53]
$NiCo_2O_4$	89	-	-	0.1 M KOH	[54]
Co_3O_4	113	-	-	0.1 M KOH	[54]
Pt/C	133	-	-	0.1 M KOH	[54]

NSs—nanosheets; NF—nickel foam; NHS—nanoheterostructure; P-NMO—phosphorized $NiMoO_4$; NMO—$NiMoO_4$; $GFC20_{800}$ and $GFC20_{700}$—gadolinium ferrite perovskite doped with divalent cation Cu^{2+}, $GdFe_{1-x}Cu_xO_3$ ($0 \leq x \leq 0.3$), calcination temperature of 800 and 700 °C, respectively.

5. Conclusions

CoM (M = Fe, Mo, Mn), Co, and Ni coatings were prepared by electroless deposition with SEM revealing somewhat different morphology. The effect of combining Co with left-hand side transition metals (Fe, Mo, Mn) on the electrocatalytic activity for water electrolysis, i.e., for both HER and OER in alkaline media, was evaluated. CoMo coating

gave the highest current densities as well as exchange current density during HER in 1 M KOH, showing a faster charge transfer through the metal–solution interface during HER. Low charge transfer resistance in the case of CoMo was confirmed by EIS analysis. Furthermore, CoMo showed the highest value of double-layer capacitance, reflecting the highest number of active sites.

On the other hand, Co and CoMn coating showed the highest current density during OER with ca. 120 mV lower overpotential to reach a current density of 10 $mA \cdot cm^{-2}$, compared to CoFe and Ni coatings. Co coating showed faster HER kinetics in terms of low Tafel slope (60 $mV \cdot dec^{-1}$) resulting from lower charge transfer resistance and higher double-layer capacitance.

Stability tests under HER as well as OER conditions in alkaline media revealed high stability of coatings studied.

Author Contributions: Conceptualization, J.M., A.B. and B.Š.; investigation, J.M., A.B., Z.S. and D.M.; data curation, J.M., A.B., D.M. and B.Š.; funding acquisition, L.T.-T.; writing—original draft preparation, J.M. and A.B.; writing—review and editing, L.T.-T., D.M.F.S. and B.Š.; visualization, J.M. and A.B.; supervision, L.T.-T. and B.Š. All authors have read and agreed to the published version of the manuscript.

Funding: The study was funded by the Ministry of Education, Science and Technological Development of Republic of Serbia (contract no. 451-03-68/2020-14/200146). The authors would also like to thank the Portuguese Foundation for Science and Technology (FCT, Portugal) for a research contract in the scope of programmatic funding UIDP/04540/2020 (D.M.F. Santos) and for contract IST-ID/156/2018 (B. Šljukić).

Institutional Review Board Statement: Not applicable.

Informed Consent Statement: Not applicable.

Data Availability Statement: The data presented in this study are available on request from the corresponding author.

Conflicts of Interest: The authors declare no conflict of interest.

References

1. Niyitanga, T.; Jeong, H.K. Hydrogen and oxygen evolution reactions of molybdenum disulfide synthesized by hydrothermal and plasma method. *J. Electroanal. Chem.* **2019**, *849*, 113383. [CrossRef]
2. Du, Y.; Wang, Z.; Li, H.; Han, Y.; Liu, Y.; Yang, Y.; Liu, Y.; Wang, L. Controllable synthesized CoP-MP (M=Fe, Mn) as efficient and stable electrocatalyst for hydrogen evolution reaction at all pH values. *Int. J. Hydrogen Energy* **2019**, *44*, 19978–19985. [CrossRef]
3. Sial, M.A.Z.G.; Baskaran, S.; Jalil, A.; Talib, S.H.; Lin, H.; Yao, Y.; Zhang, Q.; Qian, H.; Zou, J.; Zeng, X. NiCoFe oxide amorphous nanohetrostructres for oxygen evolution reaction. *Int. J. Hydrogen Energy* **2019**, *44*, 22991–23001. [CrossRef]
4. Yang, L.; Yu, G.; Ai, X.; Yan, W.; Duan, H.; Chen, W.; Li, X.; Wang, T.; Zhang, C.; Huang, X.; et al. Efficient oxygen evolution electrocatalysis in acid by a perovskite with face-sharing IrO_6 octahedral dimers. *Nat. Commun.* **2018**, *9*, 5236. [CrossRef]
5. Lv, Z.; Zhang, Y.; Wang, K.; Yu, T.; Liu, X.; Wang, G.; Xie, G.; Jiang, L. High performance of Co–P/NF electrocatalyst for oxygen evolution reaction. *Mater. Chem. Phys.* **2019**, *235*, 121772. [CrossRef]
6. Lee, C.; Lee, C.; Shin, K.; Song, T.; Jeong, H.Y.; Jeon, D.Y.; Lee, H.M. Ag_2S-CoS hetero-nanowires terminated with stepped surfaces for improved oxygen evolution reaction. *Catal. Commun.* **2019**, *129*, 105749. [CrossRef]
7. Bockris, J.O.M.; Potter, E.C. The mechanism of hydrogen evolution at nickel cathodes in aqueous solutions. *J. Chem. Phys.* **1952**, *20*, 614–628. [CrossRef]
8. Willems, H.; Kobussen, A.G.C.; De Wit, J.H.W.; Broers, G.H.J. The oxygen evolution reaction on cobalt. Part I. Reaction order experiments and impedance measurements. *J. Electroanal. Chem.* **1984**, *170*, 227–242. [CrossRef]
9. Willems, H.; Kobussen, A.G.C.; Vinke, I.C.; De Wit, J.H.W.; Broers, G.H.J. The oxygen evolution reaction on cobalt. Part II. Transient measurements. *J. Electroanal. Chem.* **1985**, *194*, 287–303. [CrossRef]
10. Lasia, A.; Rami, A. Kinetics of hydrogen evolution on nickel electrodes. *J. Electroanal. Chem.* **1990**, *294*, 123–141. [CrossRef]
11. Kawashima, A.; Akiyama, E.; Habazaki, H.; Hashimoto, K. Characterization of sputter-deposited Ni-Mo and Ni-W alloy electrocatalysts for hydrogen evolution in alkaline solution. *Mater. Sci. Eng. A* **1997**, *226–228*, 905–909. [CrossRef]
12. Neethu, R.M.; Hegde, A.C. Development of Ni-W alloy coatings and their electrocatalytic activity for water splitting reaction. *Phys. B Condens. Matter* **2020**, *597*. [CrossRef]
13. Lin, X.; Zhou, J.; Zheng, D.; Guan, C.; Xiao, G.; Chen, N.; Liu, Q.; Bao, H.; Wang, J.Q. Rational synthesis of $CaCo_2O_4$ nanoplate as an earth-abundant electrocatalyst for oxygen evolution reaction. *J. Energy Chem.* **2019**, *31*, 125–131. [CrossRef]

14. Weng, Z.; Liu, W.; Yin, L.C.; Fang, R.; Li, M.; Altman, E.I.; Fan, Q.; Li, F.; Cheng, H.M.; Wang, H. Metal/Oxide Interface Nanostructures Generated by Surface Segregation for Electrocatalysis. *Nano Lett.* **2015**, *15*, 7704–7710. [CrossRef]
15. Xu, X.; Zhong, Y.; Shao, Z. Double Perovskites in Catalysis, Electrocatalysis, and Photo(electro)catalysis. *Trends Chem.* **2019**, *1*, 410–424. [CrossRef]
16. Guan, B.Y.; Yu, L.; Lou, X.W.D. General Synthesis of Multishell Mixed-Metal Oxyphosphide Particles with Enhanced Electrocatalytic Activity in the Oxygen Evolution Reaction. *Angew. Chemie Int. Ed.* **2017**, *56*, 2386–2389. [CrossRef]
17. Gao, W.; Yan, M.; Cheung, H.Y.; Xia, Z.; Zhou, X.; Qin, Y.; Wong, C.Y.; Qu, Y.; Chang, C.R.; Ho, J.C. Modulating electronic structure of CoP electrocatalysts towards enhanced hydrogen evolution by Ce chemical doping in both acidic and basic media. *Nano Energy* **2017**, *38*, 290–296. [CrossRef]
18. Zhou, J.; Xiao, H.; Zhou, B.; Huang, F.; Zhou, S.; Xiao, W.; Wang, D. Hierarchical MoS_2-rGO nanosheets with high MoS_2 loading with enhanced electro-catalytic performance. *Appl. Surf. Sci.* **2015**, *358*, 152–158. [CrossRef]
19. Worsley, M.A.; Shin, S.J.; Merrill, M.D.; Lenhardt, J.; Nelson, A.J.; Woo, L.Y.; Gash, A.E.; Baumann, T.F.; Orme, C.A. Ultralow density, monolithic WS_2, MoS_2, and MoS_2/graphene aerogels. *ACS Nano* **2015**, *9*, 4698–4705. [CrossRef]
20. Liu, T.; Asiri, A.M.; Sun, X. Electrodeposited Co-doped $NiSe_2$ nanoparticles film: A good electrocatalyst for efficient water splitting. *Nanoscale* **2016**, *8*, 3911–3915. [CrossRef]
21. Wang, H.; Wang, X.; Yang, D.; Zheng, B.; Chen, Y. $Co_{0.85}Se$ hollow nanospheres anchored on N-doped graphene nanosheets as highly efficient, nonprecious electrocatalyst for hydrogen evolution reaction in both acid and alkaline media. *J. Power Sources* **2018**, *400*, 232–241. [CrossRef]
22. Hu, Y.; Guan, D.G.; Yu, B.; Hou, W.; Zheng, B.; Zhang, W.; Chen, Y. Scalable synthesis of Mo_2C/CNT networks as highly efficient and stable electrocatalyst for hydrogen evolution reaction. *Electrochim. Acta* **2018**, *263*, 192–200. [CrossRef]
23. Ma, F.X.; Wu, H.B.; Xia, B.Y.; Xu, C.Y.; Lou, X.W. Hierarchical β-Mo_2C Nanotubes Organized by Ultrathin Nanosheets as a Highly Efficient Electrocatalyst for Hydrogen Production. *Angew. Chemie Int. Ed.* **2015**, *54*, 15395–15399. [CrossRef]
24. Chen, P.; Xu, K.; Fang, Z.; Tong, Y.; Wu, J.; Lu, X.; Peng, X.; Ding, H.; Wu, C.; Xie, Y. Metallic Co_4N porous nanowire arrays activated by surface oxidation as electrocatalysts for the oxygen evolution reaction. *Angew. Chem. Int. Ed.* **2015**, *54*, 14710–14714. [CrossRef]
25. Ling, T.; Yan, D.Y.; Wang, H.; Jiao, Y.; Hu, Z.; Zheng, Y.; Zheng, L.; Mao, J.; Liu, H.; Du, X.W.; et al. Activating cobalt(II) oxide nanorods for efficient electrocatalysis by strain engineering. *Nat. Commun.* **2017**, *8*, 1509. [CrossRef]
26. Tahira, A.; Ibupoto, Z.H.; Willander, M.; Nur, O. Advanced Co_3O_4–CuO nano-composite based electrocatalyst for efficient hydrogen evolution reaction in alkaline media. *Int. J. Hydrogen Energy* **2019**, *44*, 26148–26157. [CrossRef]
27. Liu, H.; Yang, D.H.; Wang, X.Y.; Zhang, J.; Han, B.H. N-doped graphitic carbon shell-encapsulated FeCo alloy derived from metal–polyphenol network and melamine sponge for oxygen reduction, oxygen evolution, and hydrogen evolution reactions in alkaline media. *J. Colloid Interface Sci.* **2021**, *581*, 362–373. [CrossRef]
28. Jiang, L.; Ji, S.J.; Xue, H.G.; Suen, N.T. HER activity of M_xNi_{1-x} (M = Cr, Mo and W; x ≈ 0.2) alloy in acid and alkaline media. *Int. J. Hydrogen Energy* **2020**, *45*, 17533–17539. [CrossRef]
29. Yeo, B.S.; Bell, A.T. Enhanced activity of gold-supported cobalt oxide for the electrochemical evolution of oxygen. *J. Am. Chem. Soc.* **2011**, *133*, 5587–5593. [CrossRef]
30. Xie, S.; Li, F.; Xu, S.; Li, J.; Zeng, W. Cobalt/iron bimetal-organic frameworks as efficient electrocatalysts for the oxygen evolution reaction. *Chin. J. Catal.* **2019**, *40*, 1205–1211. [CrossRef]
31. Zhang, S.; She, G.; Li, S.; Qu, F.; Mu, L.; Shi, W. Enhancing the electrocatalytic activity of $NiMoO_4$ through a post-phosphorization process for oxygen evolution reaction. *Catal. Commun.* **2019**, *129*, 105725. [CrossRef]
32. Liang, D.; Mao, J.; Liu, P.; Li, J.; Yan, J.; Song, W. In-situ doping of Co in nickel selenide nanoflower for robust electrocatalysis towards oxygen evolution. *Int. J. Hydrogen Energy* **2020**, *45*, 27047–27055. [CrossRef]
33. Chanda, D.; Tufa, R.A.; Birdja, Y.Y.; Basu, S.; Liu, S. Hydrothermally/electrochemically decorated FeSe on Ni-foam electrode: An efficient bifunctional electrocatalysts for overall water splitting in an alkaline medium. *Int. J. Hydrogen Energy* **2020**, *45*, 27182–27192. [CrossRef]
34. Ganci, F.; Cusumano, V.; Livreri, P.; Aiello, G.; Sunseri, C.; Inguanta, R. Nanostructured Ni–Co alloy electrodes for both hydrogen and oxygen evolution reaction in alkaline electrolyzer. *Int. J. Hydrogen Energy* **2020**. [CrossRef]
35. Abbott, D.F.; Lebedev, D.; Waltar, K.; Povia, M.; Nachtegaal, M.; Fabbri, E.; Copéret, C.; Schmidt, T.J. Iridium oxide for the oxygen evolution reaction: Correlation between particle size, morphology, and the surface hydroxo layer from operando XAS. *Chem. Mater.* **2016**, *28*, 6591–6604. [CrossRef]
36. Zeradjanin, A.R.; Topalov, A.A.; Van Overmeere, Q.; Cherevko, S.; Chen, X.; Ventosa, E.; Schuhmann, W.; Mayrhofer, K.J.J. Rational design of the electrode morphology for oxygen evolution-enhancing the performance for catalytic water oxidation. *RSC Adv.* **2014**, *4*, 9579–9587. [CrossRef]
37. Eftekhari, A. From pseudocapacitive redox to intermediary adsorption in oxygen evolution reaction. *Mater. Today Chem.* **2017**, *4*, 117–132. [CrossRef]
38. Gao, M.R.; Chan, M.K.Y.; Sun, Y. Edge-terminated molybdenum disulfide with a 9.4-Å interlayer spacing for electrochemical hydrogen production. *Nat. Commun.* **2015**, *6*, 7493. [CrossRef]
39. Kong, D.; Wang, H.; Lu, Z.; Cui, Y. $CoSe_2$ nanoparticles grown on carbon fiber paper: An efficient and stable electrocatalyst for hydrogen evolution reaction. *J. Am. Chem. Soc.* **2014**, *136*, 4897–4900. [CrossRef]

40. Wang, R.; Sun, P.; Wang, H.; Wang, X. Hierarchical molybdenum carbide/N-doped carbon as efficient electrocatalyst for hydrogen evolution reaction in alkaline solution. *Int. J. Hydrogen Energy* **2018**, *43*, 17244–17251. [CrossRef]
41. Eftekhari, A. Electrocatalysts for hydrogen evolution reaction. *Int. J. Hydrogen Energy* **2017**, *42*, 11053–11077. [CrossRef]
42. Soares, C.O.; Carvalho, M.D.; Melo Jorge, M.E.; Gomes, A.; Silva, R.A.; Rangel, C.M.; Da Silva Pereira, M.I. High surface area $LaNiO_3$ electrodes for oxygen electrocatalysis in alkaline media. *J. Appl. Electrochem.* **2012**, *42*, 325–332. [CrossRef]
43. Miles, M.H. Evaluation of electrocatalysts for water electrolysis in alkaline solutions. *J. Electroanal. Chem.* **1975**, *60*, 89–96. [CrossRef]
44. Zhao, Y.; Wang, S.; Liu, H.; Guo, X.; Zeng, X.; Wu, W.; Zhang, J.; Wang, G. Porous Mo_2C nanorods as an efficient catalyst for the hydrogen evolution reaction. *J. Phys. Chem. Solids* **2019**, *132*, 230–235. [CrossRef]
45. Wang, L.; Li, Y.; Xia, M.; Li, Z.; Chen, Z.; Ma, Z.; Qin, X.; Shao, G. Ni nanoparticles supported on graphene layers: An excellent 3D electrode for hydrogen evolution reaction in alkaline solution. *J. Power Sources* **2017**, *347*, 220–228. [CrossRef]
46. Hao, Z.; Yang, S.; Niu, J.; Fang, Z.; Liu, L.; Dong, Q.; Song, S.; Zhao, Y. A bimetallic oxide $Fe_{1.89}Mo_{4.11}O_7$ electrocatalyst with highly efficient hydrogen evolution reaction activity in alkaline and acidic media. *Chem. Sci.* **2018**, *9*, 5640–5645. [CrossRef]
47. Diao, L.; Zhang, B.; Sun, Q.; Wang, N.; Zhao, N.; Shi, C.; Liu, E.; He, C. An in-plane Co_9S_8@MoS_2 heterostructure for the hydrogen evolution reaction in alkaline media. *Nanoscale* **2019**, *11*, 21479–21486. [CrossRef]
48. Yang, Y.; Fei, H.; Ruan, G.; Xiang, C.; Tour, J.M. Efficient electrocatalytic oxygen evolution on amorphous nickel-cobalt binary oxide nanoporous layers. *ACS Nano* **2014**, *8*, 9518–9523. [CrossRef]
49. Tahir, M.; Pan, L.; Idrees, F.; Zhang, X.; Wang, L.; Zou, J.J.; Wang, Z.L. Electrocatalytic oxygen evolution reaction for energy conversion and storage: A comprehensive review. *Nano Energy* **2017**, *37*, 136–157. [CrossRef]
50. Subbaraman, R.; Tripkovic, D.; Chang, K.C.; Strmcnik, D.; Paulikas, A.P.; Hirunsit, P.; Chan, M.; Greeley, J.; Stamenkovic, V.; Markovic, N.M. Trends in activity for the water electrolyser reactions on 3d M(Ni,Co,Fe,Mn) hydr(oxy)oxide catalysts. *Nat. Mater.* **2012**, *11*, 550–557. [CrossRef]
51. Du, Y.; Qu, H.; Liu, Y.; Han, Y.; Wang, L.; Dong, B. Bimetallic CoFeP hollow microspheres as highly efficient bifunctional electrocatalysts for overall water splitting in alkaline media. *Appl. Surf. Sci.* **2019**, *465*, 816–823. [CrossRef]
52. Duan, Y.; Yu, Z.; Hu, S.; Zheng, X.; Zhang, C.; Ding, H.; Hu, B.; Fu, Q.; Yu, Z.; Zheng, X.; et al. Scaled-Up Synthesis of Amorphous NiFeMo Oxides and Their Rapid Surface Reconstruction for Superior Oxygen Evolution Catalysis. *Angew. Chem.* **2019**, *131*, 15919–15924. [CrossRef]
53. Omari, E.; Omari, M. Cu-doped $GdFeO_3$ perovskites as electrocatalysts for the oxygen evolution reaction in alkaline media. *Int. J. Hydrogen Energy* **2019**, *44*, 28769–28779. [CrossRef]
54. Béjar, J.; Álvarez-Contreras, L.; Ledesma-García, J.; Arjona, N.; Arriaga, L.G. Electrocatalytic evaluation of Co_3O_4 and $NiCo_2O_4$ rosettes-like hierarchical spinel as bifunctional materials for oxygen evolution (OER) and reduction (ORR) reactions in alkaline media. *J. Electroanal. Chem.* **2019**, *847*, 113190. [CrossRef]